Image prior combination in space-variant blur deconvolution for the dual exposure problem

Miguel Tallón*, Javier Mateos*, Rafael Molina* and Aggelos K. Katsaggelos†
*Departamento de Ciencias de la Computación e I.A.
Universidad de Granada, Granada, Spain
Email: {mtallon,jmd,rms}@decsai.ugr.es
†Electrical Engineering and Computer Science Department
Northwestern University, Evanston, IL USA
Email: aggk@eecs.northwestern.edu

***Abstract*—In this paper we propose a space-variant blur estimation and effective deconvolution method when combining a long exposure blurry image with a short exposure noisy one. The blur in the long exposure shot is mainly caused by camera shake or object motion, and the noise of the underexposed image is introduced by the gain factor applied to the sensor when the ISO is set to a high value. The image pair is divided in overlapping patches for processing. The main idea in this work is to incorporate a combination of prior image models to a spatially-varying deblurring/denoising framework which is applied to each patch. The method exploits kernel and parameters estimation to choose between denoise or deblur each patch. In addition, the proposed approach estimates all necessary parameters automatically without user supervision. Experiments on both synthetic and real images validate the used approach.**

I. Introduction

The removal of the blur caused by camera shake and object motion is still a challenging problem, even more when images are taken in dim environments. A number of problems need to be addressed in single image blind deconvolution, including spatially-varying blur, and saturated pixels. Utilizing an accompanying short exposure image for the deconvolution provides valuable information that significantly improves the restoration. Unfortunately, although this additional image contains accurate information about image edges, it is generally contaminated with a high level of noise and color information might be lost.

A number of methods have been developed that use different exposure image pairs for blind deconvolution [1]–[3]. Most of the previous work assumes a space-invariant blur kernel, which seldom occurs in practice. This assumption could cause not enough blurring to be suppressed in some regions, and might lead to significant artifacts in other image parts. Recent works attempt to overcome this limitation by using space-variant blur modelling and estimation [4], or by abandoning the blur kernel estimation completely [5]. In [4], the images are divided into patches and separate blur kernels are estimated for each patch. This space-variant approach can easily lead to blocking artifacts. Furthermore, the method needs of user assistance and does not incorporates the noisy image in the restoration. In [5] a method without kernel estimation is proposed. The two images are fused into a single image by first classifying areas of the image into blurry and sharp followed by a weighted linear combination of them.

In this paper, we propose a new method to combine a long exposure blurry image with a short exposure noisy one to obtain a sharp restoration that is both noiseless and free of blur. First, we divide our input images in overlapping patches and estimate the blur kernel in each patch. We then employ a Bayesian fully-automatic procedure which combines two image priors to estimate the unknown image from the estimated kernels and the observed image pair. The proposed algorithm selectively applies deconvolution or denoising to the image patches to extract the sharp features from the image pair. Finally, the estimation of the overlapped patches is combined using a windowing function to recover a blocking-free restoration as proposed in [6]. Experimental results demonstrate that the proposed approach provides both high quality space variant blur and image estimates even in challenging datasets. The rest of paper is organized as follows. In Sec. II we describe in detail each stage of our algorithm. Synthetic and real experiments are compared and depicted in Sec. III. Finally conclusions are drawn in Sec. IV.

II. Proposed Algorithm

We assume a linear and space variant degradation model, so that the observation processes can mathematically be expressed in matrix-vector notation as

$$\mathbf{y}_1 = \mathbf{H}\mathbf{x} + \mathbf{n}_1 \quad (1)$$

$$\mathbf{y}_2 = \mathbf{x} + \mathbf{n}_2, \quad (2)$$

where $\mathbf{y}_1$ and $\mathbf{y}_2$ are the $N_y \times N_x$ observed long- and short-exposure images, respectively, represented as column vectors of size $(N_y \times N_x) \times 1$, $\mathbf{x}$ is the unknown original image, $\mathbf{n}_1$ and $\mathbf{n}_2$ are the noise components, and $\mathbf{H}$ the unknown $(N_y \times N_x) \times (N_y \times N_x)$ space-variant blur matrix.

This work was supported in part by the "Comisión Nacional de Ciencia y Tecnología" under contract TIN2010-15137 and the "Junta de Andalucía" under the contract P07-FQM-02701. Special thanks to Ramya Hebbalaguppe for the images.

Our approach to space-variant kernel estimation is summarized in the following algorithm.

Algorithm 1 Main Algorithm.

Preprocessing: image pair calibration and division in patches. (Sec. II-A)
for each patch **do**
  Perform kernel estimation, followed by kernel correction (Sec. II-B)
  Deconvolve or denoise the patch (Sec. II-C)
end for
Postprocessing: Blend the restored patches to form the final image using a windowing function (Sec. II-D)

We represent the images in the YC_bC_r colorspace. In our algorithm, the luminance component is restored and fused with the chrominance component of the blurred image. The stages of the algorithm are explained in detail in the following sections.

A. Preprocessing

The image pair with different exposure conditions must be photometrically and geometrically registered. For photometric registration, we apply histogram equalization [7] of the luminance of the short-exposure image using the histogram of the long-exposure image. The geometric calibration is performed by extracting features from both images using Surf [8] and matching them using RANSAC [9]. The quality of the restoration highly depends on the accuracy of this stage.

Then the images are divided into overlapping patches of size $B_y \times B_x$ where

$$B_z = \left\lfloor \frac{N_z}{(1-overlap)p_z + overlap} \right\rfloor, z \in \{x, y\},$$

with $0 \leq overlap < 1$ is the overlapping factor and p_x and p_y are the number of patches in the horizontal and vertical directions, respectively.

B. Kernel estimation

The space-variant kernel is estimated per patch from the observations $\mathbf{y}_1$ and $\mathbf{y}_2$. Since all following equations are applied to each patch, we use $p = (p_v, p_u)$ with $1 \leq p_v \leq p_y$ and $1 \leq p_u \leq p_x$, to refer to the specific patch (p_v, p_u). Thus $\mathbf{y}_1^p$ refers to the patch (p_v, p_u) of the long-exposure observation; equivalently $\mathbf{y}_2^p$ is the same patch in the short-exposition image. The matrix $\mathbf{Y}_2^p$ represents the image patch $\mathbf{y}_2^p$ written as a $(N_y \times N_x) \times (h_y \times h_x)$ convolution matrix, where the blur size (h_y, h_x) is provided by the user and finally, $\mathbf{h}^p$ represents the blur kernel in patch p.

Using (1) and (2), the estimate $\hat{\mathbf{h}}^p$ of a kernel $\mathbf{h}^p$ is found as

$$\hat{\mathbf{h}}^p = \min_{\mathbf{h}^p} \parallel \mathbf{y}_1^p - \mathbf{Y}_2^p \mathbf{h}^p \parallel_2^2, \quad (3)$$

subject to the constraint $0 \leq \mathbf{h}_i^p \leq 1$, $i = 1, ..., (h_x \times h_y)$.

In order to solve this constrained linear least-squares problem we use the Matlab function `lsqlin`. The boundary problem in the convolutions is solved by using the image values in the neighboring patches, when available, or by replicating the pixel values in the image borders. Since $\mathbf{y}_1^p$ and $\mathbf{y}_2^p$ are photometrically registered the constraints $\sum_i \mathbf{h}_i^p = 1$ and $\mathbf{h}_i^p \geq 0$ are generally satisfied. If that were not the case we would remove the negative values and normalize the kernel to sum up to one.

Kernel estimation may fail in patches with weak texture or saturated pixels, that is when there is not enough available information for the kernel estimation. A kernel correction algorithm is then applied. The algorithm, detailed in Alg. 2, replaces the kernel of a patch by the mean of the kernels of the neighboring patches including itself if the difference with its neighboring kernels is higher than a threshold. An alternative procedure for kernel correction is proposed in [4].

Algorithm 2 Proposed Kernel Correction Algorithm.

Input: The full space-variant kernel matrix with a kernel $\mathbf{h}^p$ per patch p.
Output: The corrected space-variant kernel matrix.
for each kernel $\mathbf{h}^p$ **do**
  Compute the mean kernel $\mathbf{h}_{mean}^p$ as the mean of $\mathbf{h}^p$ and its 8 nearest neighbor kernel patches
  Calculate $diff^p = ||\mathbf{h}^p - \mathbf{h}_{mean}^p||_1$
end for
Compute the threshold as $thr = \frac{\max(\mathbf{diff}) + \min(\mathbf{diff})}{2}$, where **diff** is the vector formed by $diff^p$, $p = 1, ..., (p_x \times p_y)$
for all kernel $\mathbf{h}^p$ such that $diff^p > thr$ **do**
  replace $\mathbf{h}^p$ by $\mathbf{h}_{mean}^p$
end for

C. Deconvolution

Once the kernel for each patch has been estimated, we need to obtain an accurate estimation of the image for each patch. In this paper we use the Bayesian deconvolution approach developed in [10] casted to our dual exposure problem.

The key idea in [10] consists of modelling, within a hierarchical Bayesian formulation, the unknown image as a combination of a sparse and a non-sparse prior models and develop a deconvolution algorithm to restore a single blurred and noisy image combining two image models. Following this approach, we will use the same image prior models, that is, a TV prior in combination with a SAR prior, and a degradation model based on (1) and (2) to model the degradations suffered by each image patch in real dim situations. We provide a description of the individual distributions used to model the unknowns in the following.

From (1) and (2), and assuming that the noise $\mathbf{n}_1$ and $\mathbf{n}_2$, in both observed patches $\mathbf{y}_1^p$ and $\mathbf{y}_2^p$, follow independent Gaussian distributions of zero mean and variances $(\beta_1^p)^{-1}$, $(\beta_2^p)^{-1}$, respectively, we write the conditional probability distribution of the observations given the unknown patch $\mathbf{x}^p$ and the noise parameters as

$$\mathrm{p}(\mathbf{y}_1^p, \mathbf{y}_2^p | \mathbf{x}^p, \beta_1^p, \beta_2^p) \propto (\beta_1^p)^{B/2} (\beta_2^p)^{B/2} \exp\left[-\frac{\beta_1^p}{2} \parallel \mathbf{y}_1^p - \mathbf{H}^p \mathbf{x}^p \parallel^2 - \frac{\beta_2^p}{2} \parallel \mathbf{y}_2^p - \mathbf{x}^p \parallel^2 \right], \quad (4)$$

where $B = B_y \times B_x$ is the number of elements of the patch.

Following the approach in [10], we propose a sparse and non-sparse models combination as image model. The sparse TV model is defined as

$$\mathrm{p}_1(\mathbf{x}^p | \alpha_1^p) \propto (\alpha_1^p)^{B/2} \exp\left[-\alpha_1^p \sum_{j=1}^{B} \sqrt{(\Delta_j^u(\mathbf{x}^p))^2 + (\Delta_j^v(\mathbf{x}^p))^2} \right], \quad (5)$$

where $j = 1, ..., B$, α_1^p is the model parameter, and the operators $\Delta_j^u(\mathbf{x})$ and $\Delta_j^v(\mathbf{x})$ correspond to horizontal and vertical first order differences at pixel j, respectively. This model provides good edges preservation but tends to smooth out textured areas. The non-sparse one, the simultaneous autoregression (SAR) model, is expected to recover more textures but smooths strong transitions as the image edges. The SAR model is defined as

$$\mathrm{p}_2(\mathbf{x}^p | \alpha_2^p) \propto (\alpha_2^p)^{B/2} \exp\left[-\frac{\alpha_2^p}{2} \parallel \mathbf{C}\mathbf{x}^p \parallel^2 \right], \quad (6)$$

where $\mathbf{C}$ is the Laplacian operator and α_2^p is the model parameter.

The proposed prior combination and observation model depends on a set of parameters whose values have to be estimated together with the image. For their modeling we employed improper non informative priors, $\mathrm{p}(\xi) \propto \text{const}$, $\xi \in \{\alpha_1^p, \alpha_2^p, \beta_1^p, \beta_2^p\}$, over $(0, \infty)$.

A variational approach is employed to obtain an approximation of the posterior distribution of the image patch and the parameters. We skip the inference stage details due to the lack of space and provide the image and parameter estimates for each patch p. The image patch $\mathbf{x}^p$ is obtained as

$$\mathbf{x}^p = \Sigma_x^p \left(\beta_1^p (\mathbf{H}^p)^t \mathbf{y}_1^p + \beta_2^p \mathbf{y}_2^p \right) \quad (7)$$

$$(\Sigma_x^p)^{-1} = \lambda \alpha_1^p \left((\Delta^u)^t \mathbf{W}^p \Delta^u + (\Delta^v)^t \mathbf{W}^p \Delta^v \right) + (1-\lambda) \alpha_2^p \mathbf{C}^t \mathbf{C} + \beta_1^p (\mathbf{H}^p)^t \mathbf{H}^p + \beta_2^p \mathbf{I}, \quad (8)$$

where Δ^u and Δ^v are the discrete approximations to the gradient operator in the horizontal and vertical directions respectively, $\mathbf{W}^p$ is the spatially varying weighting matrix that provides spatial adaptivity to the model. The parameter λ controls each prior model contribution. Thus, a value of $\lambda = 0$ leads to the classical SAR restoration model while a value of $\lambda = 1$ leads to the TV restoration model. A sensible combination of both models allows to recover the textures of the image while preserving sharp edges [10].

To select the best value of λ we found estimates of the image patch $\mathbf{x}^p$ with λ moving from 0 to 1 in steps of 0.1, and selected the value of λ and restoration $\mathbf{x}_\lambda^p$ that minimizes $\parallel \mathbf{y}_1^p - \mathbf{H}^p \mathbf{x}_\lambda^p \parallel^2$. The weights matrix $\mathbf{W}^p$ and the rest of parameter estimates are found using

$$w_j^p = (\Delta_j^u(\mathbf{x}^p))^2 + (\Delta_j^v(\mathbf{x}^p))^2 \ , j = 1, ..., B \quad (9)$$

$$\mathbf{W}^p = diag\left[\frac{1}{\sqrt{w_j^p + \epsilon}} \right] \ , j = 1, ..., B \quad (10)$$

$$\alpha_1^p = \frac{B}{2 \sum_j \sqrt{w_j^p}} \ , j = 1, ..., B \quad (11)$$

$$\alpha_2^p = \frac{B}{\parallel \mathbf{C}\mathbf{x}^p \parallel^2} \quad (12)$$

$$\beta_1^p = \frac{B}{\parallel \mathbf{y}_1^p - \mathbf{H}^p \mathbf{x}^p \parallel^2} \quad (13)$$

$$\beta_2^p = \frac{B}{\parallel \mathbf{y}_2^p - \mathbf{x}^p \parallel^2}. \quad (14)$$

To calculate $\mathbf{x}^p$ in (7) and the parameters in (9)-(14) we use the iterative procedure summarized in Alg. 3. Initializing $\mathbf{x}^p$ to $\mathbf{y}_1^p$, the long exposure image patch, and using ϵ a small positive value to avoid division by zero, we update the parameters using (9)-(14) and then, for those parameters, we calculate a new estimate of $\mathbf{x}^p$ applying a conjugate gradient method in (7). We have also experimented with other deconvolution methods such as Richardson-Lucy [11], [12] and the method in [6], but they provided results with higher amount of ringing artifacts.

Algorithm 3 Proposed Deconvolution Algorithm.

Inputs: $\mathbf{y}_1^p, \mathbf{y}_2^p$ the long- and short-exposure images patches, respectively; and $\mathbf{h}^p$ the corrected kernel estimates in patch p.
Output: $\mathbf{x}^p$ the restored patch.
for $\lambda = 0$ to 1 in steps of 0.1 **do**
  Set $\mathbf{x}_{new}^p = \mathbf{y}_1^p$
  repeat
    Set $\mathbf{x}_{old}^p = \mathbf{x}_{new}^p$
    Find the estimation of the parameters using (9)-(14) with $\mathbf{x}^p = \mathbf{x}_{old}^p$
    Find $\mathbf{x}_{new}^p$, the new image patch estimate using (7)
  until $\frac{\|\mathbf{x}_{new}^p - \mathbf{x}_{old}^p\|^2}{\|\mathbf{x}_{old}^p\|^2} \leq threshold$
  Set $\mathbf{x}_\lambda^p = \mathbf{x}_{new}^p$
end for
Set $\mathbf{x}^p = \mathrm{argmin}_{\mathbf{x}_\lambda^p} \parallel \mathbf{y}_1^p - \mathbf{H}^p \mathbf{x}_\lambda^p \parallel^2$

The proposed method results in high-quality image estimates if the blur is invariant within each patch. However, as other deconvolution algorithms, it fails to estimate the image accurately in weak textured patches and in those patches where the kernels are not invariant. A typical scenario of the latter situation is the case of object motion blur.

In the case of object motion, the algorithm has to separate the background pixels (which are not blurred) from the blurred

object in the foreground. This can be achieved by using a segmentation algorithm, but this is generally computationally unfeasible. In this paper, we work on an image patch basis, selecting for each one of the patches either the deconvolved patch or a denoised version of the noisy patch $\mathbf{y}_2^p$. Notice that due to the short exposure time of $\mathbf{y}_2$, it is expected that this observation will not be affected by motion blur. As a result, better estimations are expected by denoising $\mathbf{y}_2^p$ than by deblurring $\mathbf{y}_1^p$ in patches with inaccurate kernel estimations.

Note that in patches where the blur estimation is poor, the deconvolved patch will be quite different from the original one and the estimation of β_2 will result in a specially small value. Hence, to decide between deconvolving or denoising the patches, we compute the mean value of the estimate of β_2 for all the patches, $\bar{\beta}_2$, and apply denoising in all patches where $t * \beta_2$ is smaller than this mean value, $\bar{\beta}_2$. In our experiments we found that $t = 1.5$ is an appropriate value. Denoising is performed by the wavelets based method in [13]. This method requires the estimation of the noise variance which is obtained as the mean value of β_2^{-1} for all the blocks where deblurring is selected, that is, not taking into account the patches where $t * \beta_2 < \bar{\beta}_2$, and use it as input of the denoising method.

D. Postprocessing

In the last stage we merge all restored patches using a windowing function, win, to avoid blocking artifacts as follows

$$\mathbf{x} = \sum_{p}^{P} win^p \mathbf{x}^p \tag{15}$$

$$\sum_{p}^{P} win_k^p = 1 \text{ for } 1 \leq k \leq (N_x \times N_y), \tag{16}$$

with P the number of patches. We tried several windowing functions (Gaussian, rectangular and Hann), and found that a Hann window function over each patch, with a normalization to sum one, as proposed in [6] provided the best results.

III. Experiments

In this section we analyze the performance of the developed algorithm on synthetic and real image pairs acquired in dim environments with different digital cameras. In order to generate a synthetic dataset we apply a locally invariant blurring function to each block which leads to a globally variant blur. Assuming a locally invariant but globally variant kernel allows us to evaluate both the kernel estimation and the accuracy of the deconvolution algorithm. In all cases, we use an overlap percentage of 50%, a Hann window is used for the weights and the $threshold$ in Alg. 3 is set to 10^{-8}.

The original image in Fig. 1(a) was divided in 4×4 overlapped patches and used the kernels depicted in Fig. 3(a) to generate the blurred observation in Fig 1(b). The noisy image in Fig. 1(c) is obtained by adding white Gaussian noise of variance 458.05 to the original image (which gives a SNR of 7dB). Since for this synthetic experiment, the original image is available, we select λ for each patch p as

TABLE I
BEST VALUE OF λ FOR EACH PATCH OF THE IMAGE IN FIG. 2(D)

1	0.9	0.6	0.9
1	0.7	0.7	0.8
0.7	0.7	0.9	0.9
0.7	0.8	0.8	0.6

TABLE II
PEAK SIGNAL TO NOISE RATIO (PSNR) AND STRUCTURAL SIMILARITY (SSIM) EVALUATION MEASURES FOR THE SYNTHETIC EXPERIMENT

	PSNR	SSIM
Blurred	28.51	0.91
Noisy	21.56	0.66
Denoising [13]	32.21	0.92
Richardson-Lucy [11], [12]	29.08	0.92
Proposed method with $\lambda = 1$	32.45	0.97
Proposed method	33.33	0.97

$\text{argmin}_\lambda \parallel \mathbf{x}_{true}^p - \mathbf{x}_\lambda^p \parallel^2$ obtaining the values displayed in Table I. The other parameters were estimated from (9) to (14) using Alg. 3. Denoising was not needed to be applied to any patch of the restored image. The restoration with the proposed method depicted in Fig. 2(d) is sharper and with better textures than the denoised image depicted in Fig. 2(a). Despite the reduced size of the patches, the method recover a good kernel (see Fig. 3(b)). The RL deconvolution method, implemented by `deconvlucy` routine in Matlab, with the kernel estimates obtained in Fig. 3(b) were used for comparison. No ringing is present in the restoration with the proposed method (see Fig. 2(d)) while ringing is clearly visible when RL deconvolution is applied (Fig. 2(b)). The proposed algorithm (Fig. 2(d)) also produces better result than using TV alone (Fig. 2(c)) (obtained by setting the parameter $\lambda = 1$ for all the patches) see, for instance, the textures of the feathers which are more realistic, and the side of the nose that is smoother in our restoration and does not exhibit the typical TV piecewise effect on smooth areas. Note that the best λ for the patches including the nose is between 0.7 and 0.9. Finally, the metrics on Table II also quantitatively demonstrate the higher quality of the restoration with the proposed method.

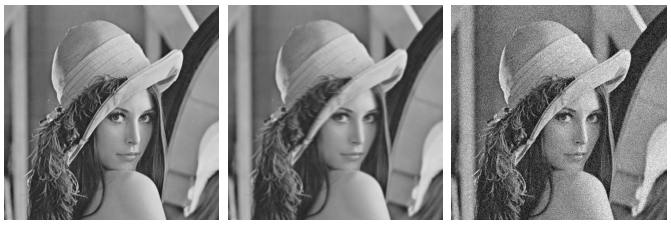

(a) (b) (c)

Fig. 1. (a) Original image, (b) blurred image with the kernels of the Fig. 3(a) and (c) observed noisy image simulating the calibrated short-exposure image.

In the next experiment, we applied the proposed method to two real image pairs, depicted in Fig. 4(a) and 4(b) and Fig. 4(d) and 4(e), acquired under dim environment with camera shake and object motion. As explained in Sec. II-A

(a) (b) (c)

(d) (e) (f)

Fig. 4. Real observed images and results of our algorithm. From left to right: observed long- and short-exposure image pair and final restoration.

the observations have been photometrically and geometrically registered before displaying. Note that histogram equalization is performed only on luminance band; however, chrominance of the dim image were also calibrated for displaying purpose only.

The experiment in the image in Fig. 4(a) shows the behavior of our algorithm for an object motion scene together with a small camera shake. The exposure time in the blurred image is 1/4s and 1/15s with exposure compensation EV -2 for the dim image, both shots with ISO 400. Since the blur is not severe, we used a kernel size of 15×15 pixels and 6×6 patches. The estimated kernel for each patch is depicted in Fig. 5(a). Although the presence of noise in the under-exposed image is low, this experiment illustrates how our algorithm is able to select the patches where the kernel is not accurately estimated due to objects motion. Note that the cyclist and the child in Fig. 4(a), both moving, are detected (see Fig. 5(b)), and replaced by the denoised, sharp versions while the rest of the image is successfully deconvolved obtaining the image displayed in Fig. 4(c).

The last experiment illustrates the behavior of our algorithm in an extremely dim indoor scene, which mixes again both, motion and camera shake blur. The exposure time in the blurred image (Fig 4(d)) is 1/8s and 1/30s with exposure compensation EV -2 for the dim image (Fig. 4(e)), both shots with ISO 400. In this experiment we used a kernel of size 21×21, and 4×4 patches. Although the blur is not severe, the estimated kernels, depicted in Fig. 5(c), show that the slight camera rotation was successfully detected by the blur estimation process, and the restoration depicted in Fig. 4(f) demonstrates the accuracy of the proposed method. Note that the blur was successfully removed from the image (see, for instance, the area of the altar in the right hand side of the image in Fig. 4(f)), and no noise from the short-exposure image was introduced in the restored image (see the column and the arch in the left hand side of Fig. 4(f)).

In all tested images the quality of the restored image is very high, providing a noise and ghost free restorations in all experiments.

IV. Conclusions

In this paper we have proposed a method to restore blurred images taken in dim environment with the help of a short-exposure crisp but noisy image. The developed algorithm can be applied to both, camera shake and object motion blur by using a space variant kernel estimation and relying on the noisy observation. The method minimizes blur artifacts and noise propagation in the recovery process. We have shown

(a) (b) (c) (d)

Fig. 2. Restorations for the synthetic images in Figs. 1(b) and 1(c): (a) denoised image, (b) RL after 35 iterations, (c) TV approach and (d) proposed method with λ values shown in Table I.

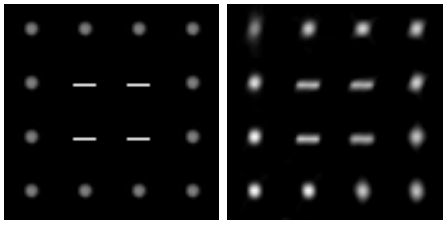

(a) (b)

Fig. 3. Spatially-variant kernel for the synthetic experiment. (a) Set of kernels used for each patch. (b) Estimated kernel for each patch.

that, using a combination of prior models into the hierarchical Bayesian paradigm, the proposed restoration method provides better results than the TV restoration method producing an image with better texture while preserving sharp edges. It is important to note that except for the size of the blur kernels, the number of patches and its percentage of overlap, all parameters are estimated automatically by the proposed method. Future work will include the use of dynamic patch size and to incorporate the estimation of the parameter λ into the Bayesian formulation.

REFERENCES

[1] L. Yuan, J. Sun, L. Quan, and H.-Y. Shum, "Image deblurring with blurred/noisy image pairs," *ACM Trans. Graph.*, vol. 26, 2007.

[2] S. D. Babacan, J. Wang, R. Molina, and A. K. Katsaggelos, "Bayesian blind deconvolution from differently exposed image pairs," *IEEE Trans. on Image Processing*, vol. 19, no. 11, pp. 2874–2888, 2010.

[3] M. Tallón, J. Mateos, S. D. Babacan, R. Molina, and A. K. Katsaggelos, "Combining observation models in dual exposure problems using the Kullback-Leibler divergence," *European Signal Processing Conference (EUSIPCO 2010)*, pp. 323–327, 2010.

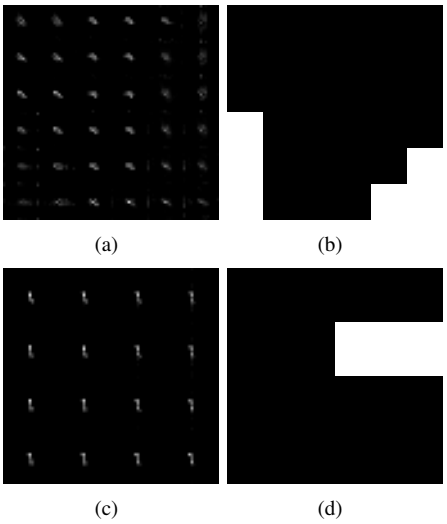

(a) (b) (c) (d)

Fig. 5. Estimated kernels and selection strategy. (a) Obtained kernels estimation for the images in Figs. 4(a) and 4(b). (b) Patches in white represent patches where denoising was applied in the restoration in Fig. 4(c). (c) Obtained kernels estimation for the images in Figs. 4(d) and 4(e). (d) Patches in white represent patches where denoising was applied in the restoration in Fig. 4(f).

[4] M. Sorel and F. Sroubek, "Space-variant deblurring using one blurred and one underexposed image," in *Proc. Int. Conf. on Imag. Proc (ICIP)*, 2009, pp. 157–160.

[5] M. Tico, N. Gelfand, and K. Pulli, "Motion-blur-free exposure fusion," in *Proc. Int. Conf. on Imag. Proc (ICIP)*, 2010, pp. 3321–3324.

[6] M. Hirsch, S. Sra, B. Scholkopf, and S. Harmeling, "Efficient filter flow for space-variant multiframe blind deconvolution," in *Proc. IEEE Conf. Computer Vision and Pattern Recognition (CVPR)*, 2010, pp. 607–614.

[7] R. C. Gonzalez and R. E. Woods, *Digital Image Processing*. Prentice Hall, 2008.

[8] H. Bay, T. Tuytelaars, and L. V. Gool, "Surf: Speeded up robust features," in *ECCV*, 2006, pp. 404–417.

[9] M. A. Fischler and R. C. Bolles, "Random sample consensus: a paradigm for model fitting with applications to image analysis and automated cartography," *Commun. ACM*, vol. 24, no. 6, pp. 381–395, 1981.

[10] M. Vega, J. Mateos, R. Molina, and A. K. Katsaggelos, "Astronomical image restoration using variational methods and model combination," *Statistical Methodology, In Press*, 2011. [Online]. Available: http://dx.doi.org/10.1016/j.stamet.2011.04.003

[11] H. W. Richardson, "Bayesian-based iterative method of image restoration," *Journal of the Optical Society of America*, vol. 62, no. 1, pp. 55–59, 1972.

[12] L. B. Lucy, "An iterative technique for the rectification of observed distributions," *Astron. J.*, vol. 79, pp. 745+, 1974.

[13] J. Portilla, V. Strela, M. J. Wainwright, and E. P. Simoncelli, "Image denoising using scale mixtures of Gaussians in the wavelet domain," *IEEE Trans. Image Processing*, vol. 12, no. 11, pp. 1338–1351, 2003.